Growth Mechanism of MoS_2 Fullerene-like Nanoparticles by Gas-Phase Synthesis

A. Zak, Y. Feldman, V. Alperovich, R. Rosentsveig, and R. Tenne*

Contribution from the Department of Materials and Interfaces, Weizmann Institute, Rehovot 76100, Israel

Received June 19, 2000

Abstract: Inorganic fullerene-like (hollow onionlike) nanoparticles (IF) and nanotubes have attracted considerable interest in recent years, due to their unusual crystallographic morphology and their interesting physical properties. IF-MoS_2 and nanotubes were first synthesized by a gas-phase reaction from MoO_3 powder. This process consists of three steps: (1) evaporation of the MoO_3 powder as molecular clusters; (2) condensation of the oxide clusters to give MoO_{3-x} nanosize particles; (3) sulfidization of the suboxide nanoparticles to generate IF nanoparticles. The evaporation of MoO_3 (step 1) and the IF particle formation from the oxide nanoparticles (step 3) have been investigated already, while the mechanism for the suboxide nanoparticles formation (step 2) has not been studied before and is reported here. According to the present model, a partial reduction of the trioxide molecular clusters (3−5 molecules) leads to the formation of MoO_{3-x} nanoparticles (5−300-nm particles size)—the precursor for IF-MoS_2. A mathematical model, which takes into account the diffusion of the reactants into the reaction zone, the chemical reactions, and the boundary conditions obtained from the experiments, is established and solved. Based on the comprehensive understanding of the IF-MoS_2 growth mechanism from MoO_3 powder and the solution of the diffusion equations, a gas-phase reactor, which allowed reproducible preparation of a pure IF-MoS_2 powder (50 mg per batch) with controllable sizes, is demonstrated.

Introduction

Condensation of molecular clusters from the vapor phase is a conventional method for nanosize particle formation. In this method, a hot vapor is quenched and entrained by a flowing inert gas. Nanoclusters are obtained by an adiabatic expansion of the vapor leading to a cooling of the clusters inert gas vapor and its condensation.[1−3] Carbon fullerenes and nanotubes were obtained by a similar synthetic process.[4]

Fullerene-related nanoparticles are derived from materials with a layered structure. Each crystallographic layer of such a nanoparticle is closed into a quasi-sphere or a tubule structure. The weak van der Waals forces between the molecular layers and the strong intralayer covalent bonds is a necessary condition for the formation of these unusual nanoparticles. There are three main types of fullerene-related particles: fullerenes (C_{60}, $C_{70,}$ etc.), nested-fullerene nanoparticles (onions), and nanotubes. Analogous fullerene-like nanoparticles were obtained from a number of inorganic materials with layered structure, which were designated as inorganic fullerene-like materials (IF).

Fullerenes are produced from carbon-rich vapor or plasma, which can be obtained using laser ablation, arc discharge, or resistive heating of graphite targets.[4−6] The synthesis of such structures implies curvature of very small atomic sheets and annihilation of the dangling bonds of the peripheral atoms. It was shown that fullerene-like nanoparticles of MoS_2 could be obtained using such methods as e-beam irradiation[7] and laser ablation[8] of regular MoS_2 powder. Short electrical pulses from the tip of a scanning tunneling microscope over a film consisting of amorphous MoS_3 nanoparticles lead to the formation of nanoparticles with a closed MoS_2 shell (IF), a few molecular layers thick, and an amorphous MoS_3 core.[9] Closed cages and nanotubes of $NiCl_2$ were recently observed upon heating $NiCl_2$ to 960 °C in a reducing atmosphere.[10] All the methods described above can be categorized as "physical"ones, since they do not exploit a chemical reaction for nanoparticle formation.

IF nanoparticles, including nanotubes, can be obtained also by "chemical" methods, in which case a chemical reaction is essential for the nanoparticles' growth. The first synthesis of IF-MS_2 (M = Mo,W) was based on the sulfidization of the respective amorphous MO_3 thin films in a reducing atmosphere at elevated temperatures (∼850 °C).[11−13] Using molybdenum oxide powder instead of a thin-film precursor, IF-MoS_2, including MoS_2, nanotubes were reported.[14] This synthesis however, resulted in miniscule amounts of the nanoparticles and a limited size control. More recently, macroscopic quantities

(1) Flagen, R. C.; Lunden, M. M. *Mater. Sci. Eng. A* **1995**, *204*, 113.
(2) Deppert, K.; Nielsch, K.; Magnusson, M. H.; Kruis, F. E.; Fissan, H. *Nanostruct. Mater.* **1998**, *10*, 565.
(3) Kruis, F. E.; Fissan, H.; Peled, A. J. *Aerosol Sci.* **1998**, *29*, 511.
(4) Dresselhaus, M. S.; Dresselhaus, G.; Eklund, P. C. *Science of Fullerenes and Carbon Nanotubes*; Academic Press: Inc.: New York, 1996; pp 1−6, 110−116.
(5) Kroto, H. W.; Heath, J. R.; O'Brien, S. C.; Curl, R. F.; Smally, R. E. *Nature* **1985**, *318*, 162.
(6) Kratschmer, W.; Lamb, L. D.; Fostiropoulos, K.; Huffman, R. *Nature* **1990**, *347*, 354.
(7) Jose-Yacaman, M.; Lorez, H.; Santiago, P.; Galvan, D. H.; Garzon, I. L.; Reyes, A. *Appl. Phys. Lett.* **1996**, *69* (8), 1065.
(8) Parilla, P. A.; Dillon, A. C.; Jones, K. M.; Riker, G.; Schulz, D. L.; Ginley, D. S.; Heben, M. J. *Nature* **1999**, *397*, 114.
(9) Homyonfer, M.; Mastai, Y.; Hershfinkel, M.; Volterra, V.; Hutchison, J. L.; Tenne, R. *J. Am. Chem. Soc.* **1996**, *118*, 33, 7804.
(10) Rosenfeld-Hacohen, Y.; Grinbaum, E.; Sloan, J.; Hutchison, J. L.; Tenne, R. *Nature* **1998**, *395*, 336.
(11) Tenne, R.; Margulis, L.; Genut, M.; Hodes, G. *Nature* **1992**, *360*, 444.
(12) Margulis, L.; Salitra, G.; Tenne, R.; Talianker, M. *Nature* **1993**, *365*, 113.
(13) Hershfinkel, M.; Gheber, L. A.; Volterra, V.; Hutchison, J. L.; Margulis, L.; Tenne, R. *J. Am. Chem. Soc.* **1994**, *116*, 1914.
(14) Feldman, Y.; Wasserman, E.; Srolovitz, D. J.; Tenne, R. *Science* **1995**, *267*, 222.

10.1021/ja002181a CCC: $19.00
Published on Web 10/28/2000

of IF-WS_2[15] and WS_2 nanotubes[16] were obtained from a powder of tungsten oxide nanoparticles. Following this early work, a few groups reported the synthesis of MoS_2 nano- and microtubes by other "chemical" methods. MoS_2 and WS_2 nanotubes were obtained by chemical vapor transport of the MS_2 powder with bromine as a transporting agent.[17,18] In an alternative approach, an aqueous solution of ammounium thiomolybdate was soaked into a porous alumina template. Subsequent annealing led to the formation of MoS_2 nanotubes, which were isolated by dissolving the alumina matrix with KOH solution.[19] More recently, sonochemical methods have been used for the synthesis of IF structures from various inorganic compounds, including Tl_2O.[20]

A model for the synthesis of IF-MS_2 (M = Mo, W) from the oxide powder was described.[15] This mechanism adequately described the growth of IF-WS_2 from WO_3 nanoparticles, but could not fully address the growth of IF-MoS_2 from MoO_3 vapor. According to this model, within the first few seconds of the reaction, an encapsulate, consisting of a skin of monomolecular MS_2 layer or two with a suboxide core, is formed. It was shown that the kinetics of the sulfidization/reduction processes on the surface of the oxide nanoparticles vary strongly with temperature.[21] Only in the temperature range 700−850 °C do the kinetics of the reaction allow sufficiently rapid generation of an absolutely closed spherical sulfide monolayer. This sulfide monolayer averts the fusion of the oxide nanoparticles into micrometer-size particles and promotes the growth of concentric spherical layers, characterizing fullerene-like structures. Later on, the suboxide core is progressively converted into IF sulfide layers by a slow diffusion-controlled reaction. *Consequently, the size and shape of the* IF *particles are determined by the size and shape of the incipient oxide nanoparticles.* It is important to note that the size of the oxide nanoparticles must not exceed 300 nm, otherwise 2H platelets of the respective sulfide are obtained.[21]

Although there are many common features in the synthesis of the IF phase of MoS_2 and WS_2, they differ in some important details. MoO_3 powder evaporates at temperatures above 700 °C, while WO_3 does not sublime below 1400 °C. Therefore, at the prevailing reaction temperatures (around 850 °C), the sulfidization of MoO_3 and WO_3 powders occurs by the gas-phase and solid−gas reactions, respectively. This means that, prior to the IF-WS_2 synthesis, the precursor oxide nanoparticles of a desirable size and shape must be prepared. In the case of IF-MoS_2, the synthetic process consists of the following three main steps: (1) evaporation of MoO_3 powder; (2) condensation of the oxide vapor to give MoO_{3-x} nanoparticles in the gas phase; (3) sulfidization of MoO_{3-x} nanoparticles in the reducing atmosphere. While steps 1 and 3 were studied before[15,21,22] in detail, step 2 was not well understood and is elucidated in the present study. Thus, the major task of the present study was to unravel the details of the growth mechanism of IF-MoS_2. As will become clear from the results below, partial reduction of the trioxide molecular clusters leads to their condensation to form suboxide nanoparticles, which serve as an intermediate in the IF-MoS_2 synthesis. This result affords a precise control over the reaction products (yield and size) and reproducible synthesis of these nanoparticles. This step is a prerequisite for a scale-up of the IF-MoS_2-phase synthesis.

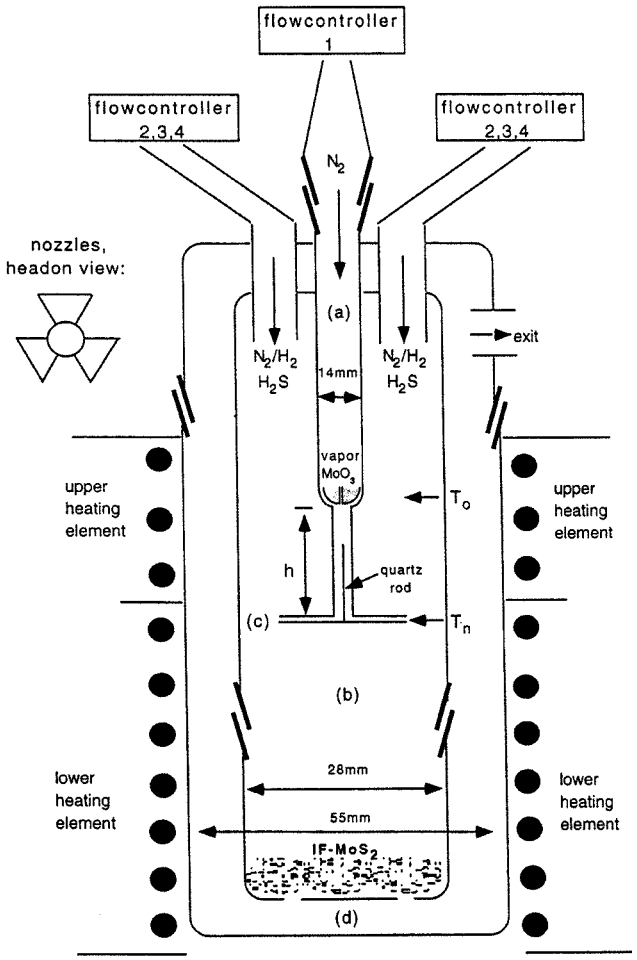

Figure 1. Schematic representation of the experimental vertical gas-phase reactor: a, inner tube; b, middle tube; c, nozzles; d, external tube.

Experimental Section

The first gas-phase synthesis of IF-MoS_2 was carried out in a horizontal reactor.[14] A mixture of N_2, H_2, and H_2S gases was made to flow through the MoO_3 vapor above a boat with trioxide powder heated to 850 °C. The products of these reactions were collected on a quartz substrate. More precise control of the reaction was achieved by separating the sublimation and sulfidization zones.[14]

Thus, a separate temperature control is required for the evaporation of the MoO_3 powder and sulfidization of the oxide nanoparticles. For this purpose, a vertically positioned two-zone oven was designed and used in these experiments.

The temperature profile of the oven was accurately determined with a precision of ±1 °C along the designed quartz reactor. The reactor, consisting of three concentric quartz tubes, is represented in Figure 1. The inner tube a served for sublimation of MoO_3 powder in the inert atmosphere of N_2. The oxide powder (∼1 g) was placed in a small bucket inside the inner tube a. The amount of oxide, evaporated in each experiment (∼100−150 mg), did not influence, appreciably, the level of the oxide in the bucket and, therefore, the rate of oxide evaporation from the bucket was time independent. For very long experiments (>4 h), the temprature of the bucket T_o was increased

(15) Feldman, Y.; Frey, G. L.; Homyonfer, M.; Lyakhovitskaya, V.; Margulis, L.; Cohen, H.; Hodes, G.; Hutchison, J. L.; Tenne, R. *J. Am. Chem. Soc.* **1996**, *118*, 5362.

(16) Rothschild, A.; Frey, G. L.; Homyonfer, M.; Tenne, R.; Rappaport, M. *Mater. Res. Innovatations* **1999**, *3*, 145.

(17) Remskar. M.; Skraba, Z.; Cleton, F.; Sanjines, R.; Levy, F. *Appl. Phys. Lett.* **1996**, *69*, 351.

(18) Remskar, M.; Skraba, Z.; Regula, M.; Ballif, C.; Sanjines, R.; Levy, F. *Adv. Mater.* **1998**, *10*, 246.

(19) Zelenski, C. M.; Dorhout, P. K. *J. Am. Chem. Soc.* **1998**, *120*, 734.

(20) (a) Mastai, Y.; Homyonfer, M.; Gedanken, A.; Hodes, G. *Adv. Mater.* **1999**, *11*, 1010. (b) Avivi, S.; Mastai, Y.; Hodes, G.; Gedanken, A. *J. Am. Chem. Soc.* **1999**, *121*, 4196. (c) Avivi, S.; Mastai, Y.; Gedanken, A. *J. Am. Chem. Soc.* **2000**, *122*, 4331.

(21) Feldman, Y.; Lyakhovitskaya, V.; Tenne, R. *J. Am. Chem. Soc.* **1998**, *120*, 4176.

(22) Berkowitz, J.; Inghram, M. G.; Chupka, W. A. *J. Chem. Phys.* **1957**, *26*, 842.

during the experiment in order to keep the evaporation rate constant. The height and size of the bucket were varied until an optimal configuration was obtained. The heated molybdenum oxide powder was sublimed and swept by the N_2 stream into the middle tube b through three small nozzles c, where the sulfidization reaction took place. The external tube d was used for the gas exit. Four electronic gas-flow controllers were used in this series of experiments. The flow rate of N_2 (J_{N_2}) in the inner tube a was controlled by flow controller 1 (see Figure 1). The other gases for this reaction were provided by flow controllers 2 (H_2S), 3 (forming gas H_2/N_2) and 4 (N_2). The forming gas was provided to the reactor in different flow rates (J_{FG}) and volume percents of hydrogen ($C_{H_2} = 1 \div 8$). The H_2S concentration (C_{H_2S}) was varied from 1 to 4%.

Finer control of the H_2 concentration was achieved by dilution of the forming gas with N_2 (flow controller 4). The gas pressure before and after each of the flow controllers was determined by manometers. A significant increase in the gas pressure after flow controller 1 was indicative of the obstruction of nozzles c by the reaction product.

The oxide evaporation temperature (T_o) was varied from 710 to 810 °C, keeping the nozzles' temperature (T_n), where the sulfidization begins, almost constant (800 ± 10 °C). The product was collected on a ceramic filter with tortuous paths. Typically, ~150 mg of MoO_3 powder was sublimed, from which only 50 mg of IF-MoS_2 was obtained as a single and isolated (pure) phase within 5−6 h. The rest of the material was transformed into various phases, which were deposited inside tube a.

The reaction products were analyzed by X-ray powder diffractometer (XRD; Rigaku Rotaflex RU-200B) with Cu Kα anode (1.541 78 Å), transmission electron microscopy (TEM; Philips model CM-120), and scanning electron microscopy (SEM; JEOL 6400), equipped with an energy-dispersion spectrometer (EDS; Link model ISIS). Samples for TEM analysis were prepared by suspending the powder in ethanol, using an ultrasonic bath, and subsequent dripping of the suspension on the grid and drying. The size of the nanoparticles was determined by TEM analysis, based on a statistics over a few hundereds nanoparticles for each sample.

Results

Various experimental parameters that influenced the reaction product were controlled in every experiment. However, it is appropriate to show here the effect of only the main parameters, such as T_n, T_o, C_{H_2}, C_{H_2S}, J_{N_2}, J_{FG}, S_n—nozzles' cross-sectional area, and h—bucket height, whose dependencies can shed light on the formation mechanism of IF-MoS_2. Thus, the dependencies of the reaction products on each parameter, which was varied around its optimum value, while keeping the others constant, will be shown.

To elaborate the growth mechanism of the nanoparticles, the reaction intermediates should be probed. Unfortunately, the present experimental setup did not permit the analysis of the gas-phase composition in situ during the reaction. However, precipitates of different colors, indicative of the oxide intermediates, were observed on the inner side of tube a.

To study the composition of these precipitates in greater detail, a thin (1 mm) and long quartz rod was inserted into the reactor and placed under the bucket in tube a (see Figure 1). This rod was easily accessible after the reaction and was analyzed by EDS. Different reduced phases of molybdenum oxide (MoO_{3-x}, MoO_2, and even metallic Mo), as well as molybdenum sulfide, were observed as separate phases on the rod, which is shown schematically in Figure 2. Molybdenum oxide is known to exist in many reduced phases MoO_{3-x} with $0 < x \leq 1$.[23] It turns out, therefore, that the reduction and sulfidization reactions of the oxide nanoparticles already occur in this tube. This means

(23) Wells, A. F. *Structural Inorganic Chemistry*; Oxford University Press: New York, 1984; pp 517−592.

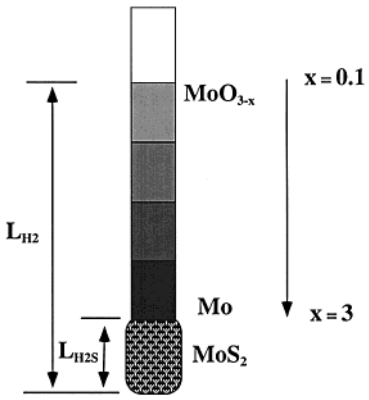

Figure 2. Schematic representation of the reaction products, which precipitated on the quartz rod, chemically identified by EDS analysis.

that both hydrogen and H_2S gases diffuse from the middle tube b into tube a against the nitrogen gas flow.

After evaporation, the MoO_3 vapors are heated-up and are carried by the J_{N_2} toward the nozzles inside tube a of the reactor. Along this path, the MoO_3 clusters are reduced by hydrogen, and they partially precipitate on the upper part of the quartz rod. EDS analysis of the precipitate indicates that the degree of reduction of the molybdenum oxide increases toward the lower part of the tube, close to the nozzles' exit c, where the hydrogen concentration is higher. The reaction of MoO_{3-x} with the diffusing H_2S gas (from b to a) leads to the formation of MoS_2 and its deposition on the lower part of the rod. The separation in space (height) between the reduction and sulfidization reactions is mainly attributed to the difference in the diffusion length of hydrogen, L_{H_2}, and H_2S, L_{H_2S}, due to the difference in the diffusion coefficient (D) of the two gases. The latter is inversely proportional to $(M)^{1/2}$, where M is the molecular weight of the gas ($M_{H_2S} = 34$; $M_{H_2} = 2$).

When strong hydrogen diffusion occurred ($L_{H_2} > h$), the MoO_3 powder inside the bucket was reduced. On the other hand, no reduction of oxide powder inside the bucket was found when the precipitation height of the suboxide was a few millimeters below the bucket height ($L_{H_2} < h$). Therefore, L_{H_2} and L_{H_2S} were determined by the precipitation height of the suboxide and the sulfide on the quartz rod. The difference in these two parameters ($L_{H_2} - L_{H_2S}$) characterizes the spatial separation between the reduction and sulfidization reactions of the MoO_3 vapor and is designated here as the "reduction volume" or "reduction path".

The relationship between L_{H_2}, L_{H_2S}, and MoO_3 vapor stream, J_{MoO_3}, on one hand, and IF-MoS_2 production (yield and size), on the other hand, as a function of the main experimental parameters, is presented here.

a. Effect of N_2 Gas Flow, J_{N_2}. The hydrogen diffusion length L_{H_2} could be varied from a few millimeters (from the nozzles' exit) to ~90 mm, which is the height of the bucket (h). The parameter that influenced L_{H_2} (and L_{H_2S}) mostly was J_{N_2} (Figure 3). Increasing J_{N_2} led to a decrease in L_{H_2} (and L_{H_2S}) and to a decrease of the IF nanoparticle sizes (see Figure 3). At a lower temperature ($T_o = 765$ °C) and higher J_{N_2}, increasing the J_{N_2} leads to a decrease in the fraction of IF phase in the product (Figure 3b). At a higher temperature ($T_o = 785$ °C) and small J_{N_2}, the yield of the IF phase remains unchanged (100%) (Figure 3a).

This figure shows also that when L_{H_2} was below ~10 mm, mostly 2H-MoS_2 platelets were obtained. The J_{N_2} had negligible influence on the evaporation rate of the MoO_3 powder under the present experimental circumstances.

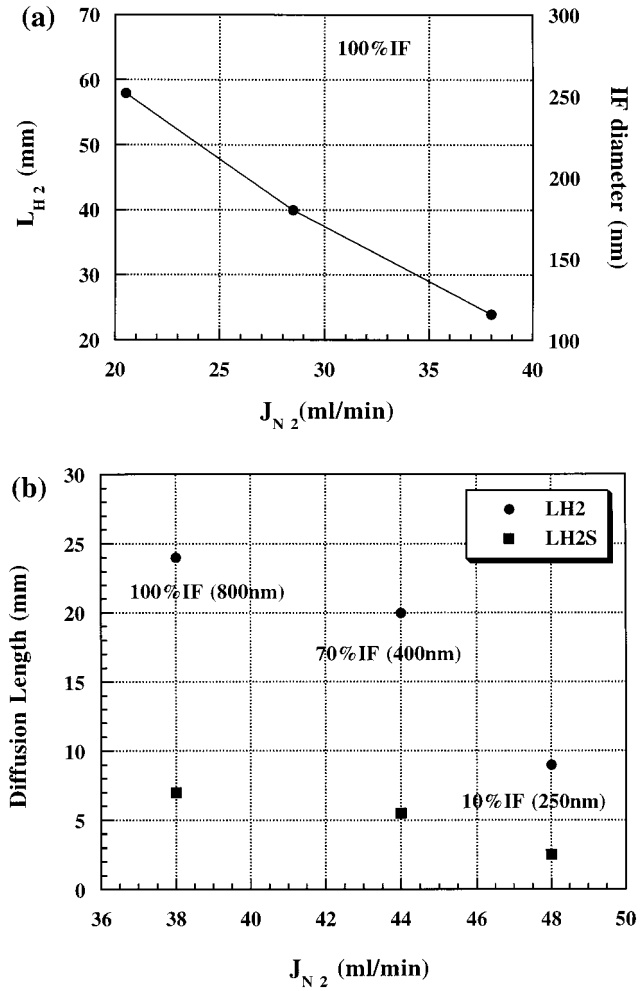

Figure 3. (a) Effect of nitrogen gas flow rate J_{N_2} on hydrogen diffusion length, L_{H_2}, and IF size. T_o = 785 °C; C_{H_2} = 5%. (b) Effect of J_{N_2} on the diffusion lengths L_{diff} (L_{H_2}, L_{H_2S}) and IF yield. T_o = 765 °C; C_{H_2} = 5%.

b. Cross-Sectional Area of the Nozzles, S_n (c in Figure 1). The effect of the nozzle cross-sectional area S_n on L_{H_2} was also rather important and can be attributed to several factors. First, according to the diffusion (Fick) law,[24] the diffusion fluxes of hydrogen and H_2S (J_{H_2} and J_{H_2S}) are linearly proportional to the cross-sectional area of the opening (nozzles). The second reason is the hydrodynamic regime of the reactor. In this reactor, two counterpropagating fluxes (J_{N_2} and J_{FG}) cross each other at the nozzle's exit (c). It was found that increasing the nozzle cross-sectional area by a factor of 2 led to an increase of L_{H_2} from 10 to 23 mm. Nonetheless, a simple relationship between S_n and IF formation was not observed, since variation in this parameter influenced many of the other experimental parameters in a nontrivial way.

Another important effect is related to the inadvertent precipitation of reduced MoO_2 in the nozzles, which tends to clog them and thereby disturb the reaction parameters. Careful matching of S_n to the kinetics of the reaction and the fluxes averted this undesirable phenomenon.

c. Hydrogen Concentration, C_{H_2}, in the Forming Gas. Increasing the hydrogen concentration in the forming gas led to an increase of L_{H_2}, while L_{H_2S} remained unchanged (see Figure 4). According to the diffusion (Fick) law,[24] the diffusion flux (J_{H_2} and J_{H_2S}) is linearly proportional to the concentration gradient. The relationship between C_{H_2} and the fraction of IF phase in the product was nonetheless found to be much more complicated. Under the specific conditions of the present series of experiments (T_o = 765 °C, J_{N_2} = 44 mL/min), increasing the hydrogen gas concentration led to an increase in the fraction of IF nanoparticles in the product. However, at lower temperatures (T_o < 720 °C), the fraction of IF nanoparticles in the product decreased with increasing C_{H_2}. This point is further discussed below.

(24) Atkins, P. W. *Physical chemistry*; Oxford University Press: New York, 1978; pp 195−222.

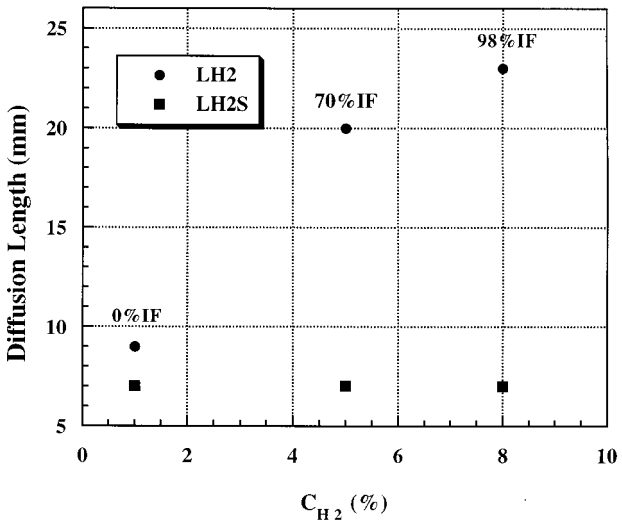

Figure 4. Effect of hydrogen concentration C_{H_2} in forming gas on hydrogen diffusion length, L_{H_2}, and IF yield. T_o = 765 °C; J_{N_2} = 44 mL/min.

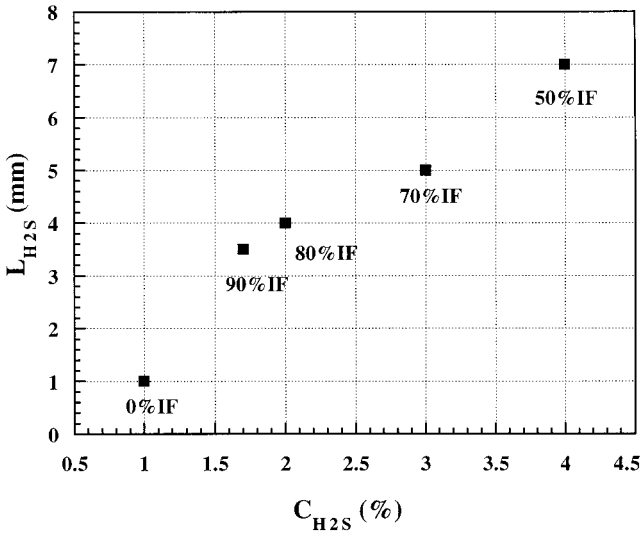

Figure 5. Effect of H_2S concentration, C_{H_2S}, in forming gas on hydrogen diffusion length, L_{H_2}, and IF yield. T_o = 725 °C; J_{N_2} = 38 mL/min; C_{H_2} = 5%.

d. Effect of H_2S Concentration, C_{H_2S}. While most of the experiments in this work were done with 4% of H_2S in the forming gas, a few experiments were carried out in lower H_2S concentrations. Figure 5 shows the effect of H_2S concentration (C_{H_2S}) on the diffusion length of the gas as determined from the height of the sulfide deposits on the quartz rod. As expected from Fick's law, a simple monotonic dependence is observed. Note also that, at these low temperatures (T_o = 725 °C), the fraction of IF-MoS_2 increases first and then decreases as the concentration of H_2S is increased.

e. Effect of Temperature. In this section, the influence of the oxide evaporation temperature, T_o, on the various fluxes is

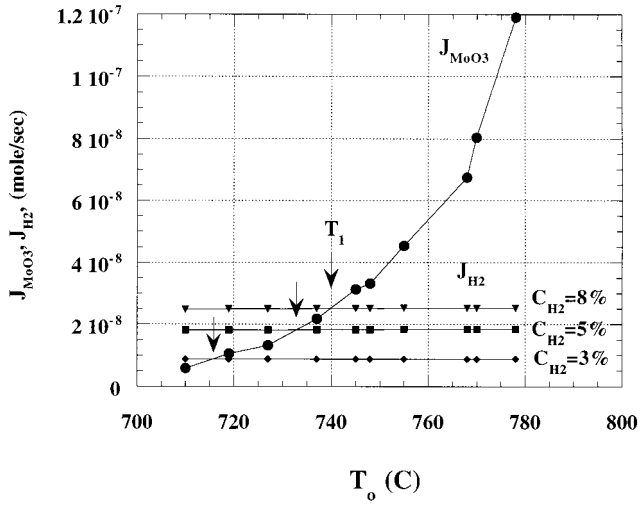

Figure 6. Molybdenum oxide evaporation rate (J_{MoO_3}) versus source temperature (T_o). Calculated hydrogen fluxes at $x = 0$ (entrance to nozzles) and $T_n = 800$ °C for different H_2 concentrations in the forming gas, are also shown.

studied. First, the temperature of the nozzles (T_n) was influenced to a minor extent, only, by varying T_o. T_n varied in the range 800 ± 10 °C, while T_o was changed between 710 and 810 °C during these experiments. Therefore, to a first approximation, the diffusion fluxes of H_2 and H_2S (J_{H_2} and J_{H_2S}) through the nozzles from (b) to (a) are taken as temperature independent in the reaction. Figure 6 shows the calculated fluxes of hydrogen in the entrance to the nozzles (c) for three different volume concentrations, as indicated (for a detailed explanation, see discussion below).

Contrarily, the MoO_3 vapor stream, J_{MoO_3} ($J_{MoO_3} = \upsilon/M$, where υ (g/s) is the evaporation rate, measured by weighing the bucket before and after the experiment, and $M = 144$, the molecular weight of MoO_3), was very sensitive to variations in the temperature (T_o). The temperature dependence of J_{MoO_3} exhibited an exponential character (Figure 6) and corresponds to the exponential dependence of the oxide vapor pressure on temperature (T_o).[23]

The highest value of J_{MoO_3}, which is obtained by the evaporation of MoO_3 powder, is a fraction of a percent of the nitrogen gas flux (J_{N_2}) in tube a. Therefore, the MoO_3 flux does not influence the hydrodynamics of the gas flow in the reactor.

Finally, the dependencies of L_{H_2S}, L_{H_2}, and IF particle size on the J_{MoO_2} (T_o) are shown in Figure 7 for two N_2 fluxes. These results are much less obvious if not counterintuitive. Most strikingly in this respect is the fact that L_{H_2} increases for increasing J_{MoO_3} (Figure 7a). It is believed that this result reflects the coalescence of the partially reduced oxide clusters into larger nanoparticles (see eq 2 below). Four different temperature zones can be discerned in this figure, reflecting the variation in IF size and yield. Zone I ($T_o = 710-725$ °C) in Figure 7a corresponds to low and constant values of L_{H_2}, where 2H-MoS_2 platelets are initially obtained. When J_{MoO_3} increases, the fraction of small IF nanoparticles (15 ± 10 nm) in the product increases (Figure 7a,b) and reaches 100% at the right-hand boundary of zone I.

In zone II (725−740 °C), the product is made of a pure IF-MoS_2 phase and L_{H_2} increased steeply with J_{MoO_3}. Simultaneously, the IF nanoparticle size increases as shown in Figure 7b. The large error bar, which is presented in Figure 7b for the particles in zone II, is due to the large size distribution, obtained from TEM analysis.

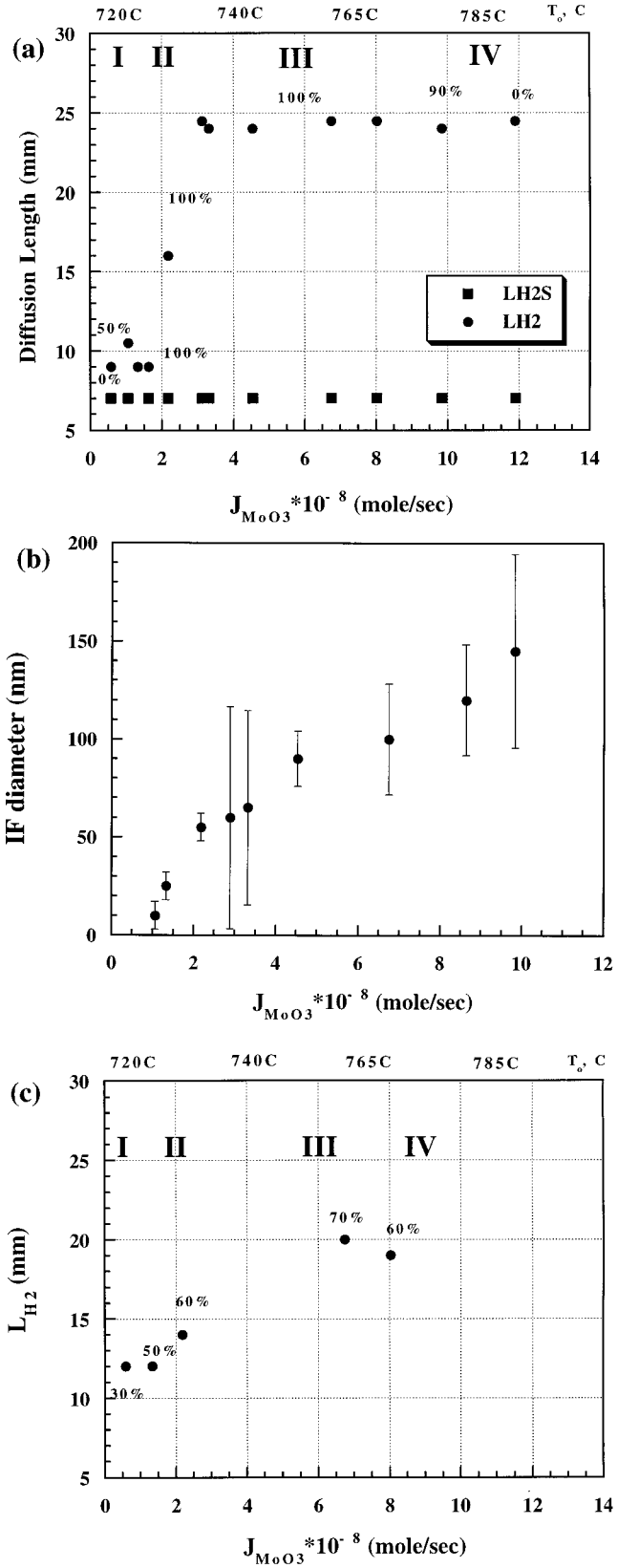

Figure 7. (a) Effect of J_{MoO_3} (T_o) on L_{diff} (L_{H_2}, L_{H_2S}) and IF yield for $J_{N_2} = 38$ mL/min. (b) IF-MoS_2 size vs J_{MoO_3} for $J_{N_2} = 38$ mL/min. (c) Hydrogen diffusion length, L_{H_2}, and IF yield vs. J_{MoO_3} for $J_{N_2} = 44$ mL/min; $T_n = 800$ °C; $C_{H_2} = 5\%$; $J_{H_2S} = 4$ mL/min.

When L_{H_2} reaches its saturation value (zone III, $T_o = 740-780$ °C), large IF nanoparticles with a relatively narrow size distribution were obtained. Subsequently, a slow increase of the IF nanoparticles size with J_{MoO_3} (Figure 7b) is observed. Note

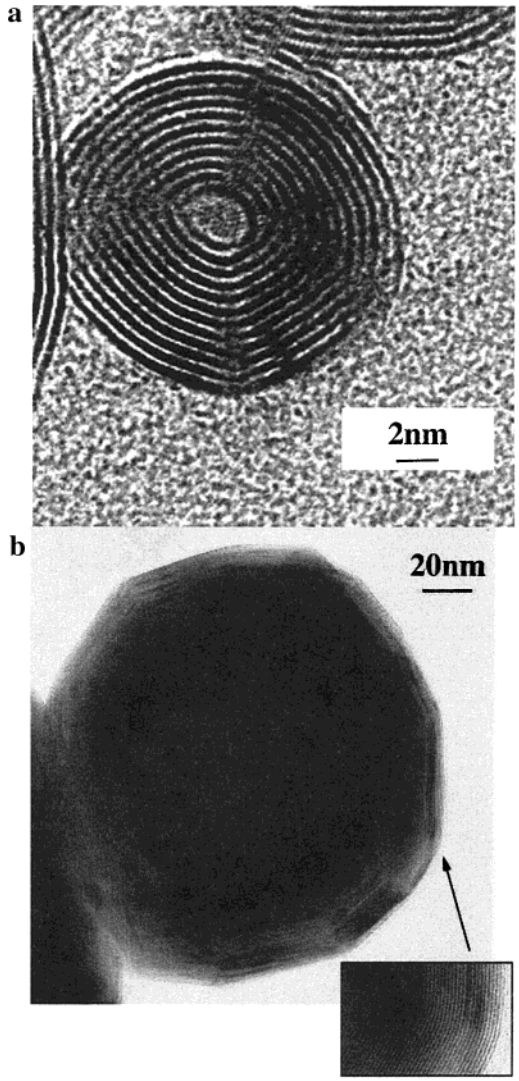

Figure 8. Typical images of IF nanoparticles with two different sizes: (a) 200 and (b) 2000 Å. The inset in (b) shows an enlarged part of the large IF nanoparticle.

that, for high values of J_{MoO_3}, the fraction of IF nanoparticles in the product decreases again (zone IV, $T_o = 780-810$ °C). When the N_2 flow is increased from 38 to 44 mL/min, the general form of L_{H_2} and IF yield vs J_{MoO_3} is preserved (Figure 7c). However, increasing the N_2 gas flow leads to a reduction in L_{H_2} and the yield, and so a pure IF phase could not be obtained under this high N_2 flux. It is to be noted that the number of experiments in this series was more limited than in Figure 7a and b.

The present study shows that full control of the production of IF nanoparticles with sizes ranging from 15 (±10) to 250 (±50) nm has been accomplished in this study. Figure 8 shows a typical image of IF nanoparticles with two different sizes.

Discussion

a. Forward. From the present results, it is clear that pure IF-MoS_2 phase with a well-defined size and relatively narrow size distribution could be obtained by this process. Variations of the nitrogen flow rate (J_{N2}), S_n, and C_{H_2} and C_{H_2S} lead to changes in L_{H_2} and L_{H_2S}, respectively, which affects the production of the IF phase. These dependencies follow the changes of J_{MoO_3}, J_{H_2}, and J_{H_2S}, which can be estimated from Fick laws (see below). The correlation between L_{H_2} (L_{H_2S}) and IF formation is not as simple. Nonetheless, it can be concluded, that the IF phase is obtained if the reduction volume ($L_{H_2} - L_{H_2S}$) is larger than some minimum value, which depends on the experimental conditions. The dependencies of L_{H_2} on J_{MoO_3} (T_o), which are shown in Figure 7, are intuitively nontrivial. The flux of H_2 propagates in the opposite direction to that of MoO_3, and an increase in J_{MoO_3} would be expected to limit the diffusion of H_2 inside tube a. Actually, an opposite behavior was observed, which cannot be explained through a linear (molecular) diffusion process.

The model proposed below intends to explain the growth mechanism for fullerene-like MoS_2 nanoparticles in the gas phase, addressing the salient experimental data.

b. Model. b.1. Chemical Processes. The first step in the synthesis of IF-MoS_2 is the evaporation of MoO_3. The vapor phase of MoO_3 consists predominantly of the molecular clusters Mo_3O_9, Mo_4O_{12}, and Mo_5O_{15}.[22] The cluster Mo_3O_9, which has a hexagonal ring structure, is the most stable one, and consequently, it is the most volatile cluster of the three. In the next step, these clusters condense into larger oxide nanoparticles.

According to the established IF growth mechanism,[15] oxide nanoparticles 5−300 nm in size are necessary as a precursor for the synthesis of IF-MoS_2.

In the present process, the temperature increases from step to step, having a positive gradient along the molecular clusters' flow. Therefore, the classical method for nanoparticle synthesis by cooling and condensation of the vapor phase[1−3] could not be invoked to explain the current growth mechanism. However, condensation can be provoked also by a chemical reaction, in which case, the vapor pressure of the product is lower than that of the precursor in the vapor phase. This mechanism was used to explain the formation of oxide nanoparticles from the $(MoO_3)_3$ clusters, in the present synthesis.

A gas-phase reaction of diffused hydrogen with Mo_3O_9 molecular clusters leads to their reduction into molybdenum suboxide. Being nonvolatile at the present working temperatures,[25] the reduced clusters condense into suboxide nanoparticles—MoO_{3-x}. Once the condensation step is completed, i.e., nanoparticles 5−300 nm in size have been obtained, they are allowed to encounter H_2S and the conversion into fullerene-like MoS_2 nanoparticles commences.[15]

A schematic representation of this process is shown in Figure 9. The reduction reaction of the vapor oxide (molecular clusters) with hydrogen (see K_1 zone, Figure 9) can be described by eq 1,

$$(MoO_3)_3 + mH_2 \xrightarrow{k_1} (MoO_{3-m/3})_3 + mH_2O \qquad (1)$$

where $m = 1, 2, 3, ..., 9$, depends on the relative concentrations of $(MoO_3)_3$ and H_2.

The coalescence of nonvolatile suboxide molecular clusters with trioxide molecular clusters is a multistep process, which results in the formation of suboxide nanoparticles (see K_2 zone, Figure 9). This multiple step reaction can be schematically represented through an apparent single step of condensation:

$$p(MoO_3)_3 + s(MoO_{3-m/3})_3 \xrightarrow{k_2} (MoO_{3-x})_n \qquad (2)$$

where $n = 3p + 3s$ are integers and $x = s(m/n)$.

The reduction process is being continued while hydrogen encounters suboxide nanoparticles (see zone K_3, Figure 9),

(25) Knacke, O.; Kubaschewski, O.; Hesselmann, K. *Thermochemical Properties of Inorganic Substances*; Springer-Verlag: Berlin, Heidelberg, 1991; pp 1264−1272.

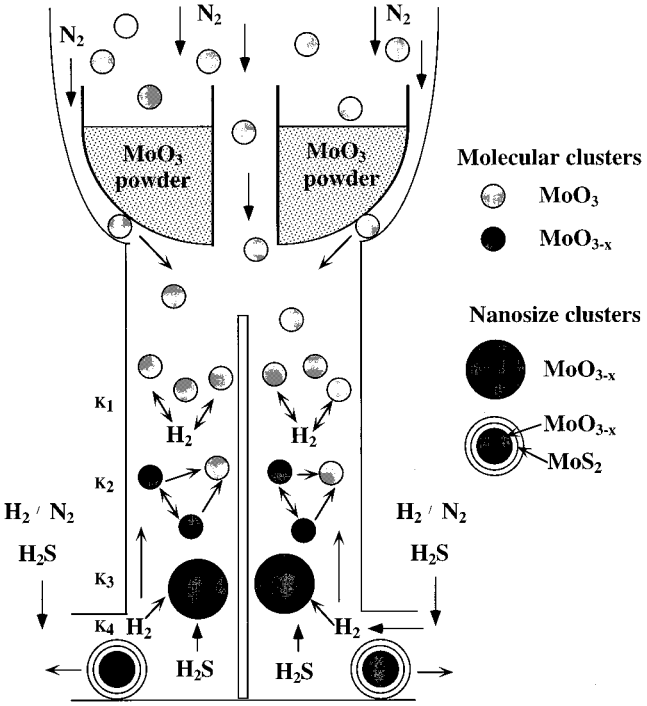

Figure 9. Scheme for the lower part of reactor a, depicting the MoO_3 evaporation, reduction, and suboxide nanoparticle formation. The sulfidization of these particles is initiated close to the nozzles' exit.

which have been formed in reactions 1 + 2.

$$(MoO_{3-x})_n + H_2 \xrightarrow{k_3} (MoO_{3-x-1/n})_n + H_2O \qquad (3)$$

The rate of reduction is proportional to the specific surface area of the nanoparticles. It was shown,[26] that the reduction rate of molybdenum oxide powder decreases substantially as a result of aggregation of the nanoparticles ($k_1 \gg k_3$). Therefore, the condensation of the molecular $(MoO_3)_3$ clusters into $(MoO_{3-x})_n$ nanosize particles inhibits their fast reduction process.

The condensed oxide nanoparticles flow to the H_2S diffusion volume, i.e., close to nozzles exit (see zone K_4, Figure 9). At this point, synthesis of IF-MoS_2 commences. The suboxide nanoparticles surrounded by a few sulfide shells (IF), flow to the filter (see Figure 1), where they are collected and continue to sulfidize. Complete conversion of the oxide nanoparticles affords hollow IF-MoS_2 after a few hours reaction:

$$(MoO_{3-x})_n + 2nH_2S + (1-x)nH_2 \xrightarrow{k_4} (MoS_2)_n + (3-x)nH_2O \qquad (4)$$

The presented model reveals that in this process the stoichiometry of the oxide precursor, synthesized in the vapor phase, is determined by the reduction and condensation reactions. Therefore, the stoichiometry of the suboxide nanoparticles depends on the relationship between the hydrogen flux (J_{H_2}) and the flux of MoO_3 (J_{MoO_3}). It is found that fullerene-like nanoparticles are obtained for $J_{H_2}/J_{MoO_3} < 1$, only.

b.2. Calculation of the Hydrogen Flux. The hydrogen stream from tube b to tube a, J_{H_2}, is determined by a diffusion and, consequently, obeys the one-dimensional Fick's laws of diffusion.[24]

$$j_{H_2}(x,t) = -D_{H_2}(\delta C_{H_2}(x,t)/\delta x) \qquad (5)$$

Since H_2 is provided to the reaction zone by diffusion, and is consumed by first-order chemical reactions (see eqs 1 and 3), the second-order Fick's equation reads

$$\delta C_{H_2}(t,x)/\delta t = D_{H_2}(\delta^2 C_{H_2}(t,x)/\delta x^2) - kC_{H_2}(t,x) \qquad (6)$$

where $j_{H_2}(x,t)$ (mol s^{-1} cm^{-2}) is the flux density of the hydrogen stream; $C_{H_2}(x,t)$ (mol/cm^3) is the H_2 concentration at a given location x at time t, D_{H_2} (cm^2/s) is the diffusion coefficient of hydrogen, $k = k_1 + k_3$, and $kC_{H_2}(t,x)$ is the rate of the chemical reaction for H_2.

The two counteracting processes, diffusion of H_2 into the reaction zone in (a) and its runoff by means of a chemical reaction with MoO_3, establish a steady state ($\delta C_{H_2}(t,x)/\delta t = 0$) of nonuniform (decreasing) H_2 concentration along the hydrogen diffusion path L_{H_2}. An appropriate equation for such time-independent process is

$$D_{H_2}(\delta^2 C_{H_2}(x)/\delta x^2) - kC_{H_2}(x) = 0 \qquad (7)$$

The solution for this equation, with the boundary conditions $C_{H_2}(x=0) = C^{o}_{H_2}$ and $C_{H_2}(x = L_{H_2}) = 0$, yields the concentration profile of H_2:

$$C_{H_2}(x) = 1.2C^{o}_{H_2}\exp[-x(k/D_{H_2})^{1/2}] - 0.2C^{o}_{H_2}\exp[x(k/D_{H_2})^{1/2}] \qquad (8)$$

Note, that $C^{o}_{H_2}$ is the H_2 concentration near the nozzles. As will be shown below, $C^{o}_{H_2}$ differs from the initial H_2 concentration in the forming gas ($C^{FG}_{H_2}$).

Substituting $L_{H_2} = (D_{H_2}/k)^{1/2}$ and eq 8 into eq 5, the hydrogen flux is obtained:

$$J_{H_2} = C^{o}_{H_2}(D_{H_2}/L_{H_2})(1.2\exp[-x/L_{H_2}] + 0.2(\exp[x/L_{H_2}]) \qquad (9)$$

In the following, J_{H_2} at the entrance to the nozzles, i.e., at $x = 0$, is calculated and compared to J_{MoO_3}. L_{H_2} is determined experimentally, as described above, and is 2.4 cm for 5% H_2 (in the forming gas). The value of D_{H_2} at 0 °C is tabulated[27] and is $D_{H_2}(0\ °C) = 0.688$ cm^2/s. The following relationship[27] was used to calculate the value of D_{H_2} at a given T_n:

$$D_{H_2} = D_{H_2}(0\ °C)((T_n + 273)/273)^{1.7} \qquad (10)$$

from which the value 6.7 cm^2/s was obtained for D_{H_2} at T_n = 800 °C.

Assuming the validity of the ideal gas relationship, $C^{FG}_{H_2}$ at the reactor temperature (T_n) is

$$C^{FG}_{H_2}(T_n) = C^{FG}_{H_2}(0\ °C)(273/(T_n + 273)) \qquad (11)$$

from which the value 5.6×10^{-7}mol/cm^3 was obtained for $C^{FG}_{H_2}$ at T_n = 800 °C and 5% hydrogen (volume percent in the forming gas). Taking into account the cross-sectional area of the three nozzles ($S_n = 0.08$ cm^2), through which the diffusion occurs, the H_2 stream is calculated to be

(26) Sloczynski, J.; Bobinski, W. *J. Solid State Chem.* **1991**, *92*, 436.

(27) Morachevski, A. G.; Sladkov, I. B. *Physical-Chemical Properties of Molecular Inorganic Compounds*'; Chimia: St. Petersburg, 1996; pp 290−293 (in Russian).

$$J_{H_2} = S_n j_{H_2} \quad (12)$$

The variation of the temperature of the nozzles (T_n) with the oxide evaporation temperature (T_o) is rather modest. Therefore, to a first approximation the diffusion flux of hydrogen from (b) to (a) is independent of the T_o. Figure 6 shows the calculated values of J_{H_2}, which are represented by straight lines. For this calculation, T_n was taken to be 800 °C and three hydrogen volume concentrations in the forming gas were considered: 3, 5, and 8%. The hydrogen diffusion is greatly influenced by the counterpropagating stream of nitrogen gas, which carries the MoO_3 clusters (see section on Effect of N_2 Gas Flow, J_{N_2}). The N_2 flux in the exit of the nozzles c is normal to the hydrogen flux (see Figure 1). Since the nozzles are narrow the outflow rate of the carrier gas from (a) to (b) is greatly increased.

Using the flow rates of J_{N_2} in (a) and J_{FG} in (b) and the cross-sectional areas of tubes a (0.08 cm^2) and b (2 cm^2), the laminar rates were calculated to be 5 and 0.5 cm/s, respectively.

The outflow of N_2 from the nozzles dilutes the hydrogen concentration in the forming gas by a factor of 10 ($C^o_{H_2} = C^{FG}_{H_2}/10$), if the mixing is completed instantaneously. In reality, the mixing is not ideal and therefore this factor is higher. A similar effect holds for the H_2S concentration. This overwhelming effect slows down the diffusion of hydrogen from (b) to (a) considerably. Another effect, which plays a much smaller role, is the dilution of the hydrogen gas by the nitrogen in the reduction volume. It can be shown that this effect reduces the effective hydrogen concentration, available for the reduction reaction by a few percent only.

The calculated hydrogen flux $J_{H_2}(x = 0)$ from this model is 1.8×10^{-8} mol/s for 5% H_2 in the forming gas.

b.3. Comparison between the Experimentally Determined J_{MoO_3} and the Calculated J_{H_2}. The bisection point (T_1) of the curves, J_{MoO_3} and J_{H_2}, in Figure 6 defines two separate zones: to the left and to the right of this point. Since the reaction between H_2 and MoO_3 molecules is very efficient, the reduction process depends on the relative fluxes of the two reactants. To the left of T_1, including T_1, $J_{H_2}/J_{MoO_3} \geq 1$, and consequently, the hydrogen excess results in a very efficient reduction of the molybdenum oxide clusters into pure MoO_2 (or metallic Mo) particles. In this case, the reaction with H_2S does not afford fullerene-like particles.[21] Consequently, 2H-MoS_2 platelets are obtained in this temperature regime. To the right of T_1, $J_{H_2}/J_{MoO_3} < 1$, and the amount of H_2 in the reaction zone is smaller than that of MoO_3. Condensation of the clusters to suboxide MoO_{3-x} nanoparticles, with subsequent IF-MoS_2 synthesis, is preferred in this regime.

As shown in Figure 6, the temperature dependence of J_{MoO_3} is appreciably stronger than that of J_{H_2}. Thus, at elevated temperatures, $J_{MoO_3} \gg J_{H_2}$. This H_2 deficiency leads to an inefficient reduction and, consequently, inefficient formation of the suboxide nanoparticles in this region. Therefore, there exists also an upper temperature threshold (T_2) for the IF phase formation. This temperature cannot be calculated from the present model and is determined experimentally, only.

Temperatures T_1 and T_2 can be varied to some extent by changing the hydrogen concentration in the forming gas and the nitrogen gas flux, which goes through tube a.

The temperature range for fullerene-like particle formation at different hydrogen concentrations was found experimentally: for $C_{H_2} = 5\% - T_1 = 725$ °C $T_2 = 785$ °C; for $C_{H_2} = 8\% - T_1 = 735$ °C $T_2 = 790$ °C and is in a good agreement with the calculated values.

As shown in Figure 6, increasing the temperature, inside the interval suitable for IF formation, leads to an increase in the ratio J_{MoO_3}/J_{H_2}, which in turn leads to bigger nanoparticles size (see Figure 7b).

c. Discussion of the Experimental Results in the Light of the Presented Model. c.1. Effect of J_{MoO_3} on the Hydrogen Diffusion Length. The presented model indicates that the condensation of molecular oxide clusters into oxide nanoparticles (eq 2) is a most crucial step in the gas-phase synthesis of IF-MoS_2. It is now used to explain the nontrivial behavior of L_{H_2} in Figure 7a.

Zone I in Figure 7a correspond to low and constant values of L_{H_2} (and L_{H_2S}). L_{H_2} is ~1 cm and L_{H_2S} is ~0.7 cm (Figure 5) in this zone. This region is also characterized by a relatively small values of J_{MoO_3} (see Figures 6 and 7). While 2H platelets are preferred on the left-hand side of zone I, IF-MoS_2 are obtained on the right-hand side of this zone. The hydrogen flux, J_{H_2}, was estimated from Fick's law (see above). It is found to be on the same order of magnitude as the lowest value of J_{MoO_3} (on the left-hand side of zone I). Therefore, on the left side of zone I there is sufficient hydrogen to reduce the molecular clusters into metallic Mo ($m = 9$ in eq 1), which reacts rapidly with H_2S.[28] Furthermore, the low density of the molybdenum oxide clusters in the reduction volume results in a low encounter probability and consequently small (<5 nm) nanoparticles. These reactions, however, are unable to produce IF-MoS_2[15,21] and the formation of platelets (2H-MoS_2) is therefore initially preferred. As the flux of MoO_3 increases in zone I, the complete reduction of the oxide clusters into metallic Mo is slowed. In addition, the density of molybdenum oxide clusters in the reduction volume increases and consequently their encounter probability becomes higher. This leads to a gradual increase in the suboxide nanoparticles size (>5 nm) and, consequently, to an increase in the fraction of the IF phase in the product, toward the right end of zone I.

Zone II is characterized by a dramatic increase of L_{H_2} (from 9 to 24 mm) and gradual increase in the (IF) nanoparticles sizes (from 20 to 100 nm) as J_{MoO_3} increases modestly from 2 to 4×10^{-8} mol/s. Note that no external parameter that could lead to an increase in L_{H_2} has been varied during this experiment.

The explanation for this nontrivial behavior can be found in the increasing rate of the condensation of the oxide clusters (eq 2) relative to their rate of reduction (eq 1). The surface area of the oxide nanoparticles, which is available for further reduction, diminishes as the particle size increases. Therefore, the overall rate of reduction (eq 3) goes down[26] and the hydrogen can propagate deeper into tube a of the reactor, i.e., increasing L_{H_2}. Thus, L_{H_2} increases while L_{H_2S} remains almost constant, leaving more time (larger reduction volume) for the small oxide clusters to be reduced and condense onto the oxide nanoparticles. This leads to coarsening of the oxide nanoparticles prior to their encounter with the H_2S gas. The larger oxide nanoparticles are characterized also by smaller deviation from stoichiometry (smaller x in eq 2), which is favorable for IF formation.[15,21] Therefore, the average size of the IF nanoparticles in the product increases in this zone (see Figure 7).

It is believed that the increase of L_{H_2} in zone II can be attributed to the condensation reaction, which is induced by the reduction of the $(MoO_3)_3$ clusters.

Zone III of Figure 7 corresponds to high and constant values of L_{H_2} and also to the disappearance of small IF nanoparticles in the product. In parallel, increasing J_{MoO_3} leads to a gradual

(28) Grange, P. *Catal. Rev.-Sci. Eng.* **1980**, *21* (1), 135.

and small increase in the IF particle size, from 100 ± 20 nm on the left-hand side of zone III to 150 ± 50 nm on the right-hand side of zone III. This indicates that in this zone the rate of reactions 2 and 3 do not vary with increasing J_{MoO_3} and consequently the IF size reaches it maximum value.

Zone IV of Figure 7 is characterized by an increase of the fraction of 2H-MoS_2 platelets to the expense of the IF nanoparticles in the product. Also, J_{MoO_3} increases exponentially, beyond a certain threshold. This effect is attributed to the large density of $(MoO_3)_3$ clusters in the vapor phase, which cannot be effectively reduced by the hydrogen gas. Therefore, the efficacy of the condensation process of the clusters into molybdenum suboxide nanoparticles diminishes.

Since the N_2 gas flow (Figure 7c) is in a direction opposite to the H_2 flux, increasing the former will lead to a slower in-diffusion of hydrogen from the tube b into the tube a. This in turn leads to a decrease in L_{H_2}, and therefore, the reduction volume shrinks and the conditions for the IF phase synthesis become less favorable. This effect is further discussed in the next section.

c.2. N_2 Flow Rate. As shown in Figure 3a,b, increasing J_{N_2} results in a decrease of L_{H_2}, L_{H_2S}, IF yield, and IF size. When J_{N_2} is very large (48 mL/min), the hydrogen diffusion length-L_{H_2} is rather small. Consequently, the reduction volume, as expressed by the reaction path $\Delta L = L_{H_2} - L_{H_2S}$ is rather small (<6 mm). The small value of ΔL does not permit a sufficient reduction of the oxide and condensation of the suboxide nanoparticles. Therefore, the amount of IF nanoparticles produced under these conditions is rather small (10%) and increases as J_{N_2} decreases (see Figure 3b). A pure IF phase is obtained when ΔL is larger than 17 mm. From now on, as ΔL increases (J_{N_2} decreases), the size of the IF nanoparticles increases. A larger reduction path allows for the reduced oxide clusters to encounter the suboxide nanoparticles for longer period of time and thereby to grow in size.

c.3. Hydrogen Concentration in the Forming Gas. In Figure 7a, a pure IF phase is obtained at 765 °C. However, if the N_2 gas flow increases from 38 to 44 mL/min (see Figures 3b and 7c), the IF phase constitutes only 70% of the total product. The deterioration of the reaction product is attributed to the reduced supply of H_2 into the reactor. Increasing the hydrogen concentration in the forming gas leads to an increase of the diffusion flux of hydrogen from (b) to (a) and to an increase in L_{H_2}, which consequently leads to an increase of the IF yield to 100%, as shown in Figure 4.

c.4. Effect of H_2S Concentration, C_{H_2S}. The influence of C_{H_2S} became perceptible at small J_{MoO_3} when L_{H_2} is low. Thus, the effect of C_{H_2S} was studied under low-temperature T_o = 725 °C, nitrogen flux (38 mL/min), and C_{H_2} = 5% and is summarized in Figure 5. Decreasing of C_{H_2S} from 4 to 1.7% leads to a decrease in L_{H_2S} (from 7 to 3.5 mm), while L_{H_2} remains unchanged (12 mm). Consequently, the reduction volume ($L_{H_2} - L_{H_2S}$) and the IF yield increased (from 5 to 8.5 mm and from 50 to 90%, respectively). An additional decline of C_{H_2S} to 1% resulted in a depletion of H_2S in tube a and the disappearance of IF in the product. It was shown[21] that the kinetics of the sulfidization/reduction processes on the surface of the oxide nanoparticles varies strongly with H_2S concentration. When the H_2S concentration is above a threshold value, the kinetics of the reaction allows sufficiently rapid generation of an absolutely closed spherical sulfide monolayer on the oxide surface. This sulfide monolayer averts the fusion of the oxide nanoparticles into micrometer-size particles and promotes the growth of concentric spherical layers, characterizing fullerene-like structures. Contrarily, for 1% C_{H_2S}, the kinetics of the sulfidization reaction is too slow, and consequently, 2H platelets are obtained, as shown on the Figure 5.

c.5. Control of the IF Particle Size. Once the reaction mechanism and the effect of the various experimental parameters were studied, rational size control of the IF nanoparticles became feasible, too. For instance, Figure 7b shows that as J_{MoO_3} (T_o) increases so do the nanoparticles' sizes (5−200 nm); Figure 3a shows that as J_{N_2} decreases the nanoparticles size increases (100−300 nm). The error bar for each J_{MoO_3} is indicative of the scattering of the particles' size in the particular synthesis.

The size of the fullerene-like nanoparticles was shown to be determined by the size of the suboxide nanoparticles.[15] In turn, the size of the suboxide nanoparticles depends on the density of the oxide molecular clusters, Mo_3O_9 (J_{MoO_3}), in the reduction volume and the size of the reduction volume ($L_{H_2} - L_{H_2S}$). Variation of these parameters permits full control of the average particle size.

It is important to emphasize that the experimental parameters are not independent of each other and in fact are highly correlated. For example, to decrease H_2 flux (J_{H_2}), one could decrease the C_{H_2} in the forming gas, but also to increase the N_2 flow rate or decrease S_n. These examples illustrate the complexity of this process and explain the great difficulty in controlling the synthesis of IF-MoS_2.

The effect of other experimental parameters on the IF particle size is more involved and was studied to some extent. IF particles as large as 300 nm could be produced, using the present technique; beyond this size, 2H platelets were favored during the growth process.

Conclusions

Taking advantage of the MoO_3 sublimation at the reaction temperature, the synthesis of IF-MoS_2 with in situ control of the particle size was elaborated. A model for MoO_{3-x} nanoparticle (>5 nm) formation from $(MoO_3)_{3-5}$ molecular clusters during the IF-MoS_2 synthesis was proposed. According to the present model, the partial reduction of $(MoO_3)_{3-5}$ molecular clusters with hydrogen leads to the formation of MoO_{3-x} nanoparticles 5−300 nm in diameter, which are the precursor for IF-MoS_2 nanoparticles. The parameters, which influence the formation of the nanoparticles are the temperature, flow rates of gases, concentrations of gases (H_2 and H_2S), and reactor construction (nozzle's size and shape, position of the oxide precursor, tube's diameter, etc).

Leaning upon the understanding of the growth mechanism of the IF-MoS_2 phase, an original gas-phase reactor was constructed that allowed a reproducible synthesis of a pure IF-MoS_2 phase (50 mg/batch) with controllable size. Based on the recent experience with IF-WS_2 nanoparticles, where understanding of the growth mechanism was a key to the successful scale-up effort to produce 20−100 g/batch,[29] the present production level of IF-MoS_2 could be further scaled-up soon.

Acknowledgment. We thank Dr. R. Popovitz-Biro for assistance with the TEM analysis and Dr. A. Fokin and Dr. G. Leitus for participating in the discussion of the diffusion model. This work was supported by grants from the Israeli Ministry of Science (Tashtiot-Strategic Research Initiative), the Israeli Academy of Sciences (Bikura-First Initiative), and Israel Science Foundation.

JA002181A

(29) Feldman, Y.; Zak, A.; Popovitz-Biro, R.; Tenne, R. *Solid State Sci.*, in press.